Int. J. Electrochem. Sci., 11 **(2016)** 9800 – 9811, doi: 10.20964/2016.12.67

International Journal of
ELECTROCHEMICAL
SCIENCE
www.electrochemsci.org

Electrochemical Properties of Cellulose Nanofiber/GrapheneNanosheet/Polyaniline Composite Film

Zirun Chen[3], *Chun Wei*[1,2,3,*], *Yongyang Gong*[1,2,3,*], *Jian Lv*[3], *Rui Du*[3]

[1] Ministry-province jointly-constructed cultivation base for state key laboratory of processing for non-ferrous metal and featured materials, Guangxi Zhuang Autonomous Region
[2] Key Laboratory of New Processing Technology for Nonferrous Metals and Materials, Ministry of Education
[3]College of Materials Science and Engineering, Guilin University of Technology, Guilin 541004, P. R. China
[*]E-mail: 1986024@glut.edu.cn, yygong@glut.edu.cn

Received: 6 September2016/ *Accepted:* 12 October 2016 / *Published:* 10 November 2016

A flexible cellulose nanofibers(CNF)/Graphenenanosheet (GNS)/polyaniline (PANI) composite film was deposited and prepared via vacuum filtration, and then the effect of GNS on the electrochemical properties of the film was studied. Morphology of the CNF/GNS/PANI film was characterized with Fourier transform infrared spectroscopy (FT-IR), Raman spectroscopy (Raman), and field emission scanning electron microscopy (FE-SEM). Moreover, with the increase of GNS content, the electrochemical properties were more evident in the first place but less evident after the GNS content reached 6 wt %. The minimum charge transfer resistance of the composite film was 1.16 Ω. The specific capacitance reached 342.87 F/g at a current density of 1 A/g. At 5 A/g, 78.92% of the capacitance was maintained after 1000 charge-discharge cycles.

Keywords:cellulose nanofiber, Graphenenanosheet ,Polyaniline , Flexible , Supercapacitor

1. INTRODUCTION

With the rapid growing demand for portable and wearable electronic devices, the development of flexible, low-cost, high performance and environmentally friendly is essential. Supercapacitors, as a novel energy-storage device with a short charging duration, long life, and high power density, are the hotspot on the resent researches[1,2]. In addition, most of researches on supercapacitors have been focus on carbon nanomaterials and conductive polymers. Graphene is a carbon material with large specific surface area, excellent electrical and thermal performance, and high mechanical

strengthwhichcan function as the electrode material in batteries[3], solar cells[4], and supercapacitors[5-7]. Conducting polymers, such as PANI(which can be easily synthesized with low-cost monomers), are considerd the most promising material because of their high pseudo-capacitance, environmental stability, and other advantages[8, 9]. Moreover, graphene has been utilized as the framework and conductive circuit in PANI electrode materials, thereby enhancing the stability and conductivity[10-15]. Among most of these reports, graphene/PANI powder was adhered to the electrode of current collector by using an adhesive (such as polytetrafluoroethylene or polyvinylidene fluoride). The doping of adhesives has a negative impact on the composition and electrical conductivity of the electrode.

CNF is a green and renewable nano-material with high strength, small density, biocompatibility and other characteristics. It has been widely used in paper-reinforcing agent, photoelectric composite materials, fuel cells, biomaterials and medical materials[16-19]. Moreover, it can strong bind with carbon nanofillers or conductive polymers and introduces the excellent properties of CNF to the composite [20-22]. Currently, composites between CNF and graphene, conductive polymers, and CNT, for the preparation of the electrode material of flexible supercapacitors, have been reported[18, 23-25]. Herein, we prepared the CNF/graphene/PANI composite film which free from binder for the electrode material in supercapacitors. In the composite, CNF, PANI, and GNS were the substrate, conductive medium, and reinforcement material, respectively. The effect of GNS on the electrochemical performance of the film was further investigated.

2. EXPERIMENTAL SECTION

2.1 Materials

GNS (0.2-1 μm in diameter; 20 nm in thickness) was purchased from Maoxing Technical Development Co., Ltd., Shanghai City. Sisal pulp was home-made. Sodium chloroacetate was obtained from Huihong Composite Materials Co., Ltd., Suzhou City. Ethanol (EtOH), ammonium persulfate (APS), aniline, sodium hydroxide (NaOH), hydrochloric acid (HCl), and sulfuric acid (H2SO4) were obtained from Xilong Chemical Co., Ltd., Shantou City.

2.2 Preparation of CNF/GNS/PANI composite film

According to the literature[26], PANI was prepared as follows: 7.5 mL of aniline was the added to 250 mL of hydrochloric acid (1 mol/L, aq). 4.5 g of APS was added to another equivalent HCl solution. Both solutions were mixed and stirred for 1 min. 5 h later, the product was rinsed with EtOH and deionized water 5 times, and diluted with deionized water to obtain a PANI solution.

CNF was prepared with the sisal pulp via grafting method with sodium chloroacetate[27] as follows: 1.5 g of NaOH was dissolved in 85 wt % EtOH (aq). 6 g of bleached sisal pulp was added. At 75 ºC, 1.847 g of sodium chloroacetate was added. The oxidation reaction exceeded for 3 h with stirring. The raw product was rinsed with deionized water 5 times and filtered. Then, the product was

diluted with deionized water to obtain a 0.45 wt % CNF solution with stirring for 10 min at 10000 rpm, with a JK-818IIstirrer.

The CNF/GNS/PANI composite film was prepared via the filtration–deposition method (Fig.1). 257 mg of the GNS powder and 227.65 g of the CNF solution were dispersed in deionized water with ultrasound for 30 min, with a 500 W KW-500DB ultrasonic device. 130.096 g of the PANI solution (1.977 wt %) was added to the mixture. After stirred at 10000 rpm for 10 min, an CNF/GNS/PANI dispersion was obtained. The dispersion was filtrated at vacuum and a flexible CNF/GNS/PANI composite film was deposited (Fig.2).

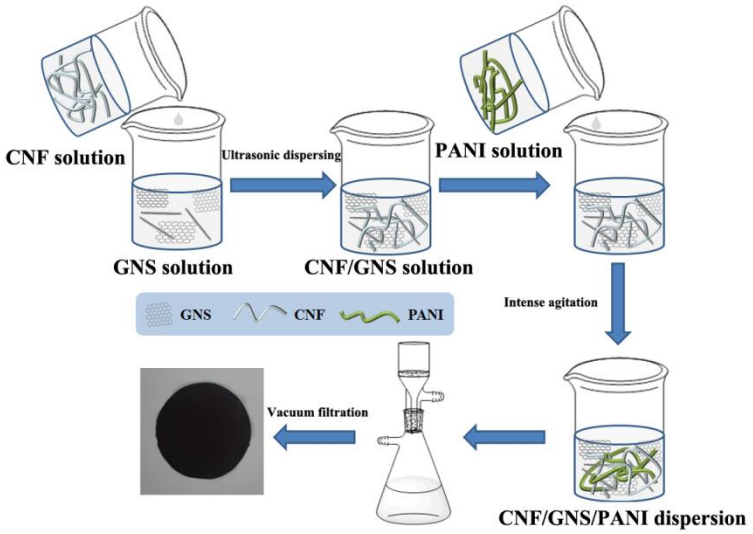

Figure 1. Schematic synthesis process of the CNF/GNS/PANI composite film.

Figure 2. Photographs of the flexible CNF/GNS/PANI composite film.

2.3 Characterizations

Functional groups were analyzed with Fourier transform infrared spectroscopy (FT-IR) by using a NICOLETNEXU 470 infrared spectrometer (Perkin-Elmer Co., Ltd., USA) with a resolution

of 4 cm^{-1} and Raman spectroscopy (Raman) with a 532 nm He-Ne ray (Thermo Fisher Scientific DXR; Thermo Electron Corporation, USA). A JSM6380-LV field emission scanning electron microscope (FE-SEM; JEOL Co., Ltd., Japan) was used to observe the morphology of product at an accelerating voltage of 3 kV.

2.4 Electrochemical test of the CNF/GNS/PANI composite film

The electrochemical properties were tested with the three-electrode system in a CHI690I electrochemical workstation (Chen Hua Co., Ltd., Shanghai City), with 1 M sulfuric acid (aq) as the electrolyte. The three-electrode system was composed of a Pt electrode (counter electrode), Ag/AgCl electrode (reference electrode), and the composite material (working electrode). The working electrode was manufactured with the composite film (1 cm × 1 cm) on a stainless steel substrate (1 cm × 4 cm) through tabletting at 10 MPa for 20 s.

The electrochemical properties were also tested with cyclic voltammetry (CV) at a scan rate of 10 to 200 mv/s. Galvanostatic charge/discharge test (GCD) was performed in the voltage range of 0 to 0.8 V and current-density range of 1 to 5 A/g. Electrochemical impedance spectroscopy (EIS) was performed in the frequency range of 0.01 to 100 kHz, with an amplitude of 0.005 V.

3. RESULTS AND DISCUSSION

3.1 Morphology and structure of the CNF/GNS/PANI composite film

3.1.1 SEM characterization

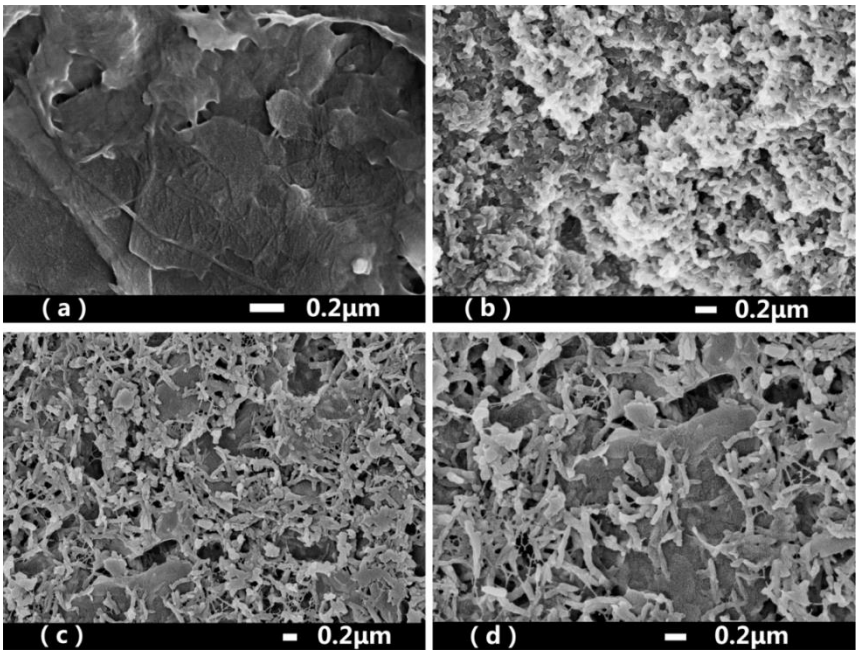

Figure 3. SEM images of (a) the CNF/GNS film, (b) pure PANI powder, and (c-d) the CNF/GNS (6 wt %)/PANI film.

FE-SEM of the film, prepared with the CNF/GNS solution, is shown in Fig.3a. CNF was uniformly distributed on the surface of GNS, with a diameter of 50 to 100 nm. GNS was effectively peeled and uniformly dispersed. In contrast, pure nano-PANI-wire was shown in Fig.3b, and long-chained PANI, with a diameter of 50 to 100 nm, was assembled.

As illustrated in Fig.3c and d, after the CNF/GNS solution was mixed with the PANI solution with vigorous stirring, PANI and CNF were entangled and uniformly dispersed on the surface and surroundings of GNS, resulting in a strong interaction between GNS, CNF, and PANI. In addition, the vigorous stirring, together with the interaction, prohibited the agglomeration of PANI.

3.1.2 FT-IR spectroscopy

FT-IR spectra of CNF, GNS, PANI, CNF/PANI, and CNF/GNS/PANI composite films are depicted in Fig.4. The CNF curve at 898, 1061, 1374, 1424, 2903, and 3345 cm^{-1}, the deformation-vibration peak of C1–H, skeletal vibration peak of the C–O–C pyranose ring, deformation vibration peak of –OH, deformation vibration peak of –CH2, stretching vibration peak of C–H, characteristic band of hydroxyl were observed respectively[27].

As illustrated in the GNS curve, at 1635, 1400, and 1176 cm^{-1}, the vibration peak of a benzene ring, bending-vibration peak of –OH, and stretching-vibration peak of secondary alcohols were observed respectively, indicating that, after the physical peeling, the GNS was still partially coated with residual hydroxyls, which functioned as the channels for the migration of ions to the inside. The residual hydroxyls contributed to the wetness of electrode materials[28].

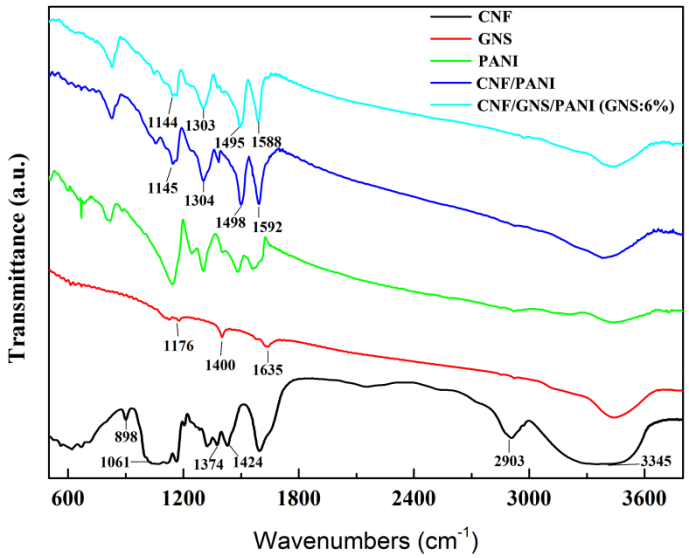

Figure 4. FT-IR spectra of CNF, GNS, PANI, CNF/PANI, and CNF/GNS/PANI films.

In the CNF/PANI curve, the peaks at 1592, 1498, 1304, and 1145 cm^{-1} correspond to quinone ring, stretching-vibration of N=C=N, stretching-vibration of C–N, and bending of C–H in the quinone ring, respectively, in accordance with the functional groups in PANI. In the CNF/GNS/PANI curve,

the afore-mentioned peaks in the CNF/PANI curve at 1592, 1498, and 1304 cm^{-1} were shifted to 1588, 1495, and 1303 cm^{-1}, respectively. And, the intensity of these peaks was significantly decreased, indicating strong hydrogen-bonding and π-π interactions between GNS, PANI and CNF.

3.1.3 Raman spectroscopy

Raman results of CNF, GNS, PANI, CNF/PANI, and CNF/GNS/PANI are illustrated in Fig.5. In the CNF curve, the peaks at 1080, 1386, and 2900 cm^{-1} are attributed to the asymmetrical-stretching of glycoside link, deformation-vibration of $–CH_2$, and stretching-vibration of $–CH_2$, respectively. This is consistent with the Raman spectrum of CNF in the literature[29].

In the GNS curve, the peaks at 1349 and 1580 cm^{-1} are the so-called D and G peaks, respectively. The ratio between the intensity of D peak and intensity of G peak (I_D/I_G=0.61) indicates that the content of defects in the GNS was low. In addition, the peak at 2700 cm^{-1} corresponds to the 2D peak of GNS[30]. In the CNF/PANI curve, the peaks at 1483, 1412 and 1161 cm^{-1} correspond to the stretching-vibration of C=N in the quinone ring, vibration of C–N in the benzene and quinone rings, and vibration of C–H in the quinone ring, respectively. These results agree with the characteristic peaks of PANI[12, 14]. In the presence of GNS, the peaks of CNF/GNS/PANI composite were shifted (red-shift) from 1349, 1580, 2700 cm^{-1} to 1345, 1577, and 2698 cm^{-1}, respectively. And, the intensity was significantly increased, indicating that CNF, GNS and PANI were strongly interacted, consistent with the SEM and FT-IR results.

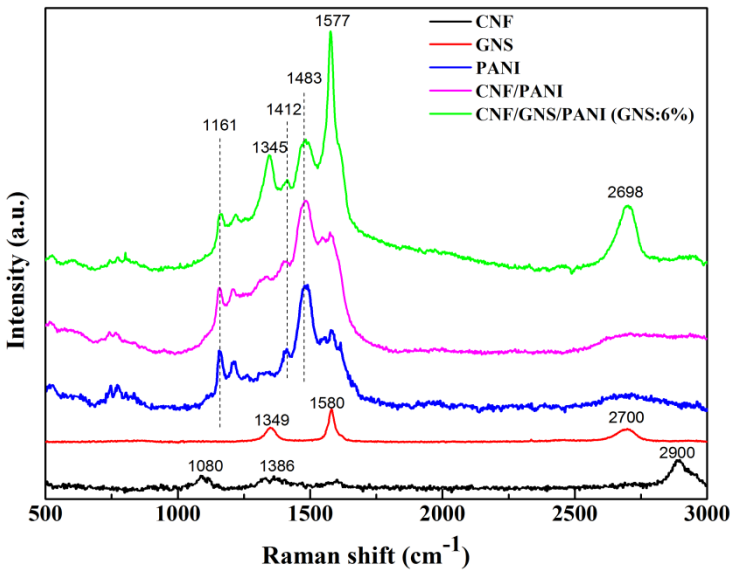

Figure 5. Raman spectra of CNF, GNS, PANI, CNF/PANI, and CNF/GNS/PANI films.

3.2 Effect of GNS content on the electrochemical performance of the CNF/GNS/PANI film

The electrochemical properties were characterized with CV, GCD, EIS, and cycling stability test.

3.2.1 CV curve

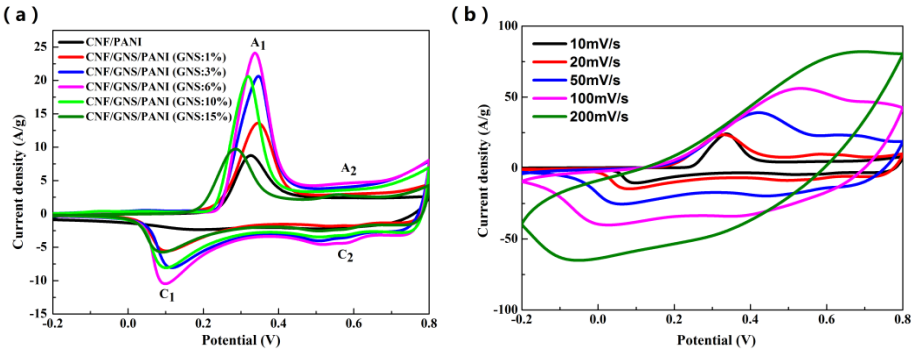

Figure 6. CV profiles of (a) CNF/GNS/PANI composite films at 10 mV/s and (b) CV profiles of CNF/GNS (6 wt %)/PANI composite film at different scan rates.

In Fig.6a, two pairs of redox peaks (A_1/C_1 and A_2/C_2) were observed in the CNF/GNS/PANI composite, wherein A_1/C_1 was ascribed to the redox transition between the conductor state and semiconductor state of PANI. A_2/C_2 was assigned to the benzoquinone and aminoquinone pairs[30], indicating that the composite film was a typical pseudo-capacitor.It is also clear observed that the current density and surround by CV curves of CNF/GNS/PANI composite is larger than that of CNF/PANI, which indicate that the synergistic effect between GNS and PANI could improve the electrochemical properties. Moreover, the loops of CNF/GNS(6wt%)/PANI composite film are larger than that of CNF/PANI composite film and any GNS ratios of CNF/PANI/GNS composite film. It means that the well dispersion of GNS and PANI could form a conductive network which can ensures the maximum utilization of PANI[14], and exhibits higher capacitance.

Fig.6b shows the CV curves of CNF/GNS(6 wt %)/PANI composite film at different scan rates.it can be seen that the reduction peaks(C1/C2) shift negatively and the oxidation peaks(A1/A2) shift positively with an increase scan rates from 10-200mV/s, which due to the resistance of electrode increase at a high scan rate[11]. In addition, the CV curves of CNF/GNS (6 wt %)/PANI composite film tended to be more stable and symmetrical at a higher scan rate, and the current density, resulting from the redox, increased dramatically, indicating that this film had good rate capability.

3.2.2 GCD curve

Further, the effect of GNS on the electrochemical performance of the CNF/GNS/PANI film was characterized with GCD at a current density of 1 A/g. As shown in Fig.7a, the GCD curves were isosceles-triangle-shaped, indicating a great capacitive behavior[30].

The specific capacitance versus GNS content was illustrated in Fig.7b, which was calculated based on the data in Fig.7a, according to the equation $Cs=I/(m(\Delta V/\Delta t))$,where I in amperes, m in grams, ΔV in volts and Δt in second represent the test current, the mass of the electrode material, the voltage range and the discharge time, respectively[31]. It can be obviously observed that the specific capacitances of CNF/GNS/PANI composite film are much higher than that of CNF/PANI composite

film, revealing the introduction of GNS could greatly improve the electrochemical performance of CNF/PANI composite film due to the synergistic effect of GNS and PANI[12]. Moreover, the CNF/GNS(6 wt%)/PANI composite film show the highest specific capacitance(342.87F/g) which are about 1.68 times higher than CNF/PANI composite film(203.63F/g) and superior to those of CNF/MWCNTs/PANI composite film (207.2F/g) fabricated by in situ chemical polymerization, 3D hollow ball of graphene and PANI hybrid (331F/g at 1A/g) fabricated by self-assembly and PANI/nylon naonofiber reinforced cellulose acetate composite film (402F/g at 0.3A/g) fabricated by in situ polymerization[32-34]. It can be explained by two main reason. Firstly, the best dispersion of GNS lead to the strong interaction between GNS and PANI, and greatly enhance the double-layer capacitance of CNF/GNS(6 wt%)/PANI composite film. Secondly, the hollow among GNS can contain the electrolyte and provide a shorter charge-transfer path, thus facilitate the electron transfer[14,30].The GCD results of CNF/GNS (6 wt %)/PANI film at different current densities (1–5 A/g) are shown in Fig.7c. These curves were still isosceles-triangle-shaped. It is demonstrated that in the wide range the film was stable and sustainable.

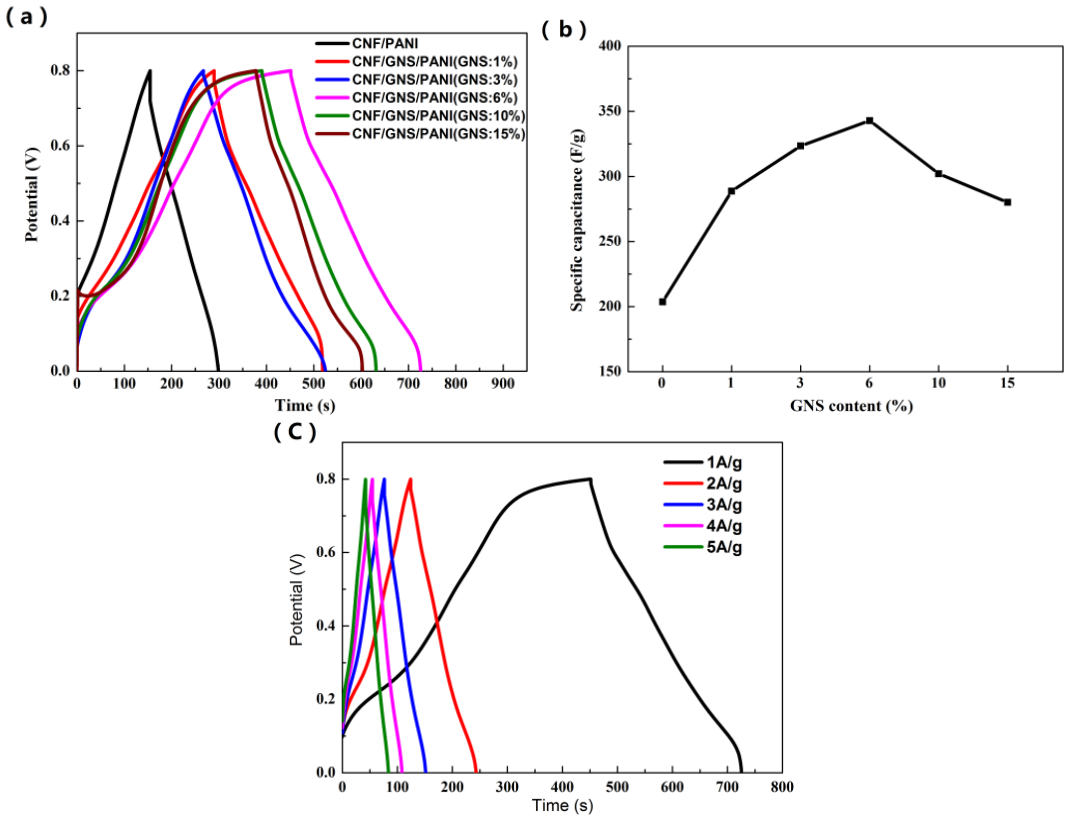

Figure 7. GCD profiles of (a) CNF/GNS/PANI composite films at 1 A/g, (b) specific capacitances of these films versus GNS content (wt %) at 1 A/g, and (c) GCD profiles of CNF/GNS (6 wt %)/PANI film at different current densities

3.2.3 EIS curve

The electrochemical impedance in Fig.8 can predict the specific capacitance and charge-transfer performance of the film. With the Zview2.0 software, the semicircular portion of the EIS

curve was fitted. the diameter of semicircle in the Nyquist plots represented the charge transfer resistance (Rct) which determine the factors limiting the performance of an electrode, charge-transfer properties[24]. It can be easily observed that the Rct value of CNF/GNS(6 wt%)/PANI(1.16 Ω) was smaller than the CNF/PANI composite film and any GNS ratio of CNF/GNS/PANI composite film, indicate that the CNF/GNS(6 wt%)/PANI composite film has fast diffusion of ions and well permeation of electrolyte, which may attributed to the gaps between GNS sheet and the strong interaction between GNS and PANI. Moreover, The CNF/GNS(6 wt%)/PANI composite film shows a nearly vertical line on Nyquist plots that means it exist a pseudocapacitive and EDLC behavior[6].

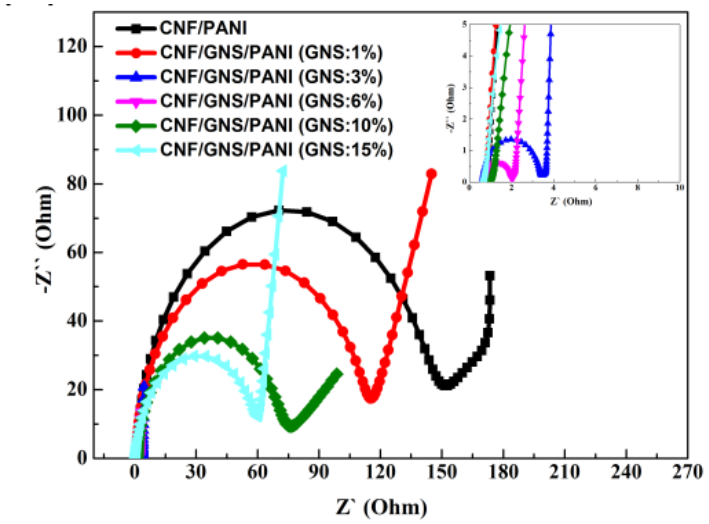

Figure 8. EIS profiles of CNF/GNS/PANI composite films

3.2.4 Cycling stability curve

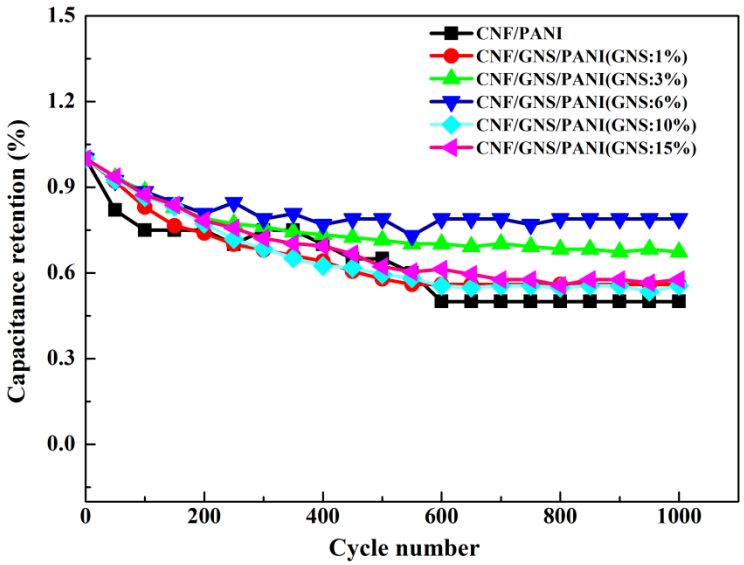

Figure 9. Cycling stability of CNF/GNS/PANI films with different GNS contents (wt %) at 5 A/g.

The influence of GNS content on the cycling performance of the CNF/GNS/PANI film is shown in Fig.9.The CNF/GNS(6 wt%)/PANI composite film exhibits a stable cycling life and keeps 78.92% of the initial capacitance after 1000 cycles at a current density of 5A/g. while the CNF/PANI composite film almost 49.49% being lost after 1000 charge-discharge cycles, which attributed to the shrinking and swelling of PANI during the charge-discharge progress[35]. The excellent cycling stability of CNF/GNS(6 wt %)/PANI composite film is mainly due to the GNS was regularly oriented under vacuum filtration, which can effectively restricting the shrinking and swelling of PANI during cycling process. Besides, the hole between GNS can absorb the electrolyte and shorter the transfer length of electron[36], thus the rate performance improved.

Furthermore, the cross-section SEM images of CNF/GNS/PANI films with different GNS contents are illustrated in Fig.10a–c. As shown in Fig.10a, PANI was stacked in thick layers, which was caused by the vacuum filtration, thus reducing the space and channels for the free migration of ions [37].

In Fig.10b, GNS in the film (6 wt % GNS) was regularly oriented. The voids between the oriented GNS sheets were favorable to the absorption of the electrolyte and provided channels for the diffusion of ions. Therefore, the migration time of the ions would be shortened because the transfer resistance was reduced. In Fig.10c, an excess of GNS would be stacked, which reduced the number of channels and hence caused the declined electrochemical performance.

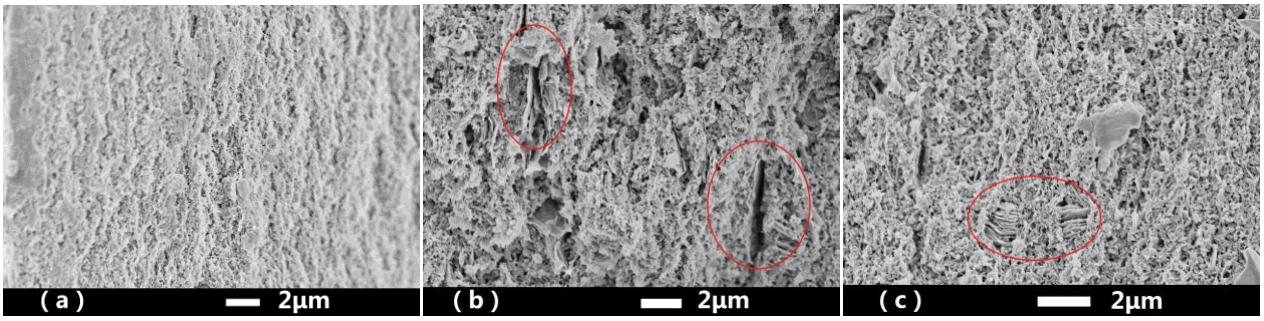

Figure 10. Cross-sections of (a) CNF/PANI film, (b) CNF/GNS (6 wt %)/PANI film, and (c) CNF/GNS (15 wt %)/PANI film.

4. CONCLUSION

Flexible CNF/GNS/PANI composite films were prepared via vacuum filtration. The presence of GNS improved the electrochemical properties of CNF/PANI film. At the GNS content of 6 wt %, GNS inside the CNF/GNS (6 wt %)/PANI film was oriented to form voids between the GNS sheets. The voids were favorable to the migration of ions and the electrochemical properties. At the current density of 1 A/g, the specific capacitance of the CNF/GNS (6 wt %)/PANI film reached a maximum of 342.87 F/g. Simultaneously, the electron transfer resistance was as low as 1.16 Ω. 78.92% of the specific capacitance was maintained after 1000 cycles at a current density of 5 A/g. This flexible, low-cost composite film may be considered as a potential material for flexible supercapacitors.

ACKNOWLEDGEMENTS
The authors would like to acknowledge the National Natural Science Foundation of China (Grant No. 21264005), Guangxi Natural Science Foundation of China (Grant No.: 2014GXNSFAA118321), Foundation of Guangxi Ministry-Province Jointly-Constructed Cultivation Base for State Key Laboratory of Processing for Non-ferrous Metal and Featured Materials (13AA-6).

References

1. P. Simon and Y. Gogotsi, *Nat. Mater.*, 7 (2008) 845.
2. W. K. Chee, H. N. Lim, Z. Zainal, N. M. Huang, I. Harrison and Y. Andou, *J. Phys. Chem. C*, 120 (2016) 4153.
3. F. Ye, B. T. Zhao, R. Ran and Z. P. Shao, *J. Power Sources*, 290 (2015) 61.
4. N. Yang, J. Zhai, D. Wang, Y. Chen and L. Jiang, *ACS Nano*, 4 (2010) 887.
5. J. J. Yoo, K. Balakrishnan, J. Huang, V. Meunier, B. G. Sumpter, A. Srivastava, M. Conway, A. L. Mohana Reddy, J. Yu, R. Vajtai and P. M. Ajayan, *Nano Letters*, 11 (2011) 1423.
6. V. Sahu, S. Shekhar, R. K. Sharma and G. Singh, *ACS Applied Materials & Interfaces*, 7 (2015) 3110.
7. Y. Ma, W. Chen, P. Zhang, F. Teng, J. Zhou, X. Pan and E. Xie, *RSC Advances*, 4 (2014) 47609.
8. Z.X. Chen and H.B. Lu, *Chemical Journal of Chinese Universities*, (2013) 2020.
9. V. H. R. de Souza, M. M. Oliveira and A. J. G. Zarbin, *J. Power Sources*, 260 (2014) 34.
10. A. Khosrozadeh, M. A. Darabi, M. Xing and Q. Wang, *Acs Applied Materials & Interfaces*, 8 (2016) 11379.
11. T. Fan, S. Tong, W. Zeng, Q. Niu, Y. Liu, C.-Y. Kao, J. Liu, W. Huang, Y. Min and A. J. Epstein, *Synth. Met.*, 199 (2015) 79.
12. Q. Liu, L. Liu, K. Xie, Y. Meng, H. Wu, G. Wang, Z. Dai, Z. Wei and Z. Zhang, *Journal of Materials Chemistry A*, 3 (2015) 8380.
13. M. A. Q. Xue, F. W. Li, J. Zhu, H. Song, M. N. Zhang and T. B. Cao, *Adv. Funct. Mater.*, 22 (2012) 1284.
14. J. Luo, Q. Ma, H. Gu, Y. Zheng and X. Liu, *Electrochimica Acta*, 173 (2015) 184.
15. N. A. Kumar, H.-J. Choi, Y. R. Shin, D. W. Chang, L. Dai and J.-B. Baek, *ACS Nano*, 6 (2012) 1715.
16. B. M. Cherian, A. L. Leao, S. F. de Souza, S. Thomas, L. A. Pothan and M. Kottaisamy, Cellulose Nanocomposites for High-Performance Applications, *Springer Berlin Heidelberg*, (2011) Berlin, Heidelberg, Germany.
17. X. Shi, A. Lu, J. Cai, L. Zhang, H. Zhang, J. Li and X. Wang, *Biomacromolecules*, 13 (2012) 2370.
18. Z. Shi, G. O. Phillips and G. Yang, *Nanoscale*, 5 (2013) 3194.
19. H.-J. Kim, H.-J. Kwon, S. Jeon, J.-W. Park, J. Sunthornvarabhas and K. Sriroth, Electrical and Optical Properties of Nanocellulose Films and Its Nanocomposites, *Springer Berlin Heidelberg*, (2015) Berlin, Heidelberg, Germany.
20. M. Park, D. Lee, S. Shin, H.-J. Kim and J. Hyun, *Carbohydrate Polymers*, 140 (2016) 43.
21. N. Song, D. Jiao, P. Ding, S. Cui, S. Tang and L. Shi, *Journal of Materials Chemistry C*, 4 (2016) 305.
22. J. V. Edwards, N. Prevost, K. Sethumadhavan, A. Ullah and B. Condon, *Cellulose*, 20 (2013) 1223.
23. K. Devarayan, D. Y. Lei, H. Y. Kim and B. S. Kim, *Chem. Eng. J.*, 273 (2015) 603.
24. Y. Liu, J. Zhou, J. Tang and W. Tang, *Chemistry of Materials*, 27 (2015) 7034.
25. K. Gao, Z. Shao, J. Li, X. Wang, X. Peng, W. Wang and F. Wang, *Journal of Materials Chemistry A*, 1 (2013) 63.
26. X. Shi, L. Zhang, J. Cai, G. Cheng, H. Zhang, J. Li and X. Wang, *Macromolecules*, 44 (2011) 4565.
27. C. Eyholzer, N. Bordeanu, F. Lopez-Suevos, D. Rentsch, T. Zimmermann and K. Oksman,

Cellulose, 17 (2010) 19.
28. L. F. Lai, H. P. Yang, L. Wang, B. K. Teh, J. Q. Zhong, H. Chou, L. W. Chen, W. Chen, Z. X. Shen, R. S. Ruoff and J. Y. Lin, *Acs Nano*, 6 (2012) 5941.
29. M. O. Adebajo, R. L. Frost, J. T. Kloprogge and S. Kokot, *Spectrochimica Acta Part A: Molecular and Biomolecular Spectroscopy*, 64 (2006) 448.
30. S. Wang, L. Ma, M. Gan, S. Fu, W. Dai, T. Zhou, X. Sun, H. Wang and H. Wang, *J. Power Sources*, 299 (2015) 347.
31. Y. Xie, Y. Liu, Y. Zhao, Y. H. Tsang, S. P. Lau, H. Huang and Y. Chai, *Journal of Materials Chemistry A*, 2 (2014) 9142.
32. C. Yang and D. G. Li, Mater. Lett., 155 (2015) 78.
33. N. B. Trung, T. V. Tam, H. R. Kim, S. H. Hur, E. J. Kim and W. M. Choi, *Chem. Eng. J.*, 255 (2014) 89.
34. K. Devarayan, D. Y. Lei, H. Y. Kim and B. S. Kim, *Chem. Eng. J.*, 273 (2015) 603.
35. H. Yan, K. Tomizawa, H. Ohno and N. Toshima, *Macromol. Mater. Eng.*, 288 (2003) 578.
36. W. Dai, L. Ma, M. Gan, S. Wang, X. Sun, H. Wang, H. Wang and T. Zhou, *Materials Research Bulletin*, 76 (2016) 344.
37. C. Yang, C. Chen, Y. Pan, S. Li, F. Wang, J. Li, N. Li, X. Li, Y. Zhang and D. Li, *Electrochimica Acta*, 182 (2015) 264.